Pergamon

Int. J. Solids Structures Vol. 35, No. 16, pp. 1863–1880, 1998

0020-7683/98 $19.00 + .00

PII: S0020-7683(97)00163-4

HIERARCHIC FINITE ELEMENTS FOR THIN NAGHDI SHELL MODEL

C. CHINOSI, L. DELLA CROCE and T. SCAPOLLA
Dipartimento di Matematica, Università di Pavia, Via Abbiategrasso, 209, I-27100 Pavia, Italy
E-mail: terenzio@dragon.ian.pv.cnr.it

(*Received* 6 *August* 1996; *in revised form* 16 *May* 1997)

Abstract—Two approaches have traditionally been used when general shell structures have been analysed. The first approach has been devised by Kirchhoff and Love and later the model has been improved by Koiter. A second class of models is based on the notion of surface introduced by Cosserat. Naghdi has developed this model, where the Reissner–Mindlin-type assumptions are taken into account. In this paper we consider the shell model arising from the Naghdi formulation. It is known that finite element schemes for this model suffer from both shear and membrane locking. Several solutions to avoid the numerical locking have been proposed. Here a displacement finite element scheme is developed using C^0 finite elements of hierarchic type with degrees ranging from one to four. Two severe test problems are solved. The results show that good performances are achieved by using high-order finite elements to solve the shell problem in its displacement formulation. The numerical results indicate that high-order elements perform very well in both test problems and match all the available benchmark results. © 1998 Elsevier Science Ltd.

1. INTRODUCTION

Several shell structures abound in nature, so it is not surprising that these efficient structural forms have been used in many engineering works. It is well known that a shell is a three-dimensional structure where one dimension, the thickness, is smaller compared with the remaining two dimensions. It can be derived from a thin plate by initially forming the middle plane to a curved surface. Under the action of external forces the shell, initially at rest, is subject to deformation according to the laws of the three-dimensional elasticity. Although the same assumptions regarding the transverse distribution of strains and stresses are again valid, the way in which the shell supports external loads is quite different from that of a flat plate.

As in the case of the plate bending model, even a shell model can be derived according to different physical assumptions. When the fibers are supposed to keep normal to the middle surface after deformation, i.e. the Kirchhoff hypothesis is assumed, the Koiter's model is obtained (Koiter, 1970). When the normals to the undeformed middle plane remain straight, but not necessarily normal to the deformed middle surface, i.e. the Reissner–Mindlin hypothesis is assumed, another family of models is obtained (Naghdi, 1963, 1972; Bathe, 1982; Hughes, 1987; Zienkiewicz, 1991).

The internal energy of the shell is the sum of the bending energy and the membrane energy in the Koiter's model. With the Reissner–Mindlin assumptions, the energy due to transverse shear appears as well. As regards the numerical analysis of the Koiter model we refer to Bernadou and Boisserie (1982), where they prove the existence and the uniqueness of the solution of the approximate problem. An overview of the main results is also given in Bernadou (1994).

In the finite element approximation of shell models with Reissner–Mindlin assumptions, two distinct classes of shell elements emerge:

- degenerate shell elements based on three-dimensional continuum theory;
- shell elements founded on the classical shell theory.

The degenerate solid approach is described firstly in the paper of Ahmad *et al.* (1970). The works of Ramm (1977), Bathe and Dvorkin (1986), and Liu *et al.* (1966), among many

others, are representative of such an approach. The degenerate solid approach discretizes the fundamental equations of a three-dimensional continuum introducing simultaneously physical assumptions at discrete points, usually applied in shell theory. Typical of this approach is the isoparametric interpolation. Stresses and strains are analysed in a local or global orthogonal Cartesian co-ordinate system, thus following the continuum-like approach.

The second afore-mentioned methodology represents a return to the origins of classical shell theory, which has its modern point of departure in the pioneering work of Cosserat (1909), further elaborated upon by a number of authors (Naghdi, 1972; Antman, 1976; Simo *et al.* 1989a, 1989b, 1990b). The basic assumption of this theory is that the midsurface of the shell is regarded as an inextensible one-director Cosserat surface. The underlying kinematic assumptions associated with this description of the shell are the usual Reissner–Mindlin hypothesis. Typical of this approach is the exact analytical definition of the initial geometry of the shell and the representation of the stress and strain state in curvilinear coordinates.

It is known that, despite its simple approach, the discretization of the Reissner–Mindlin model is not straightforward both in plates and shells frames. The inclusion of transverse shear strain in the finite element models introduce an undesirable numerical effect, the so called shear locking phenomenon. Consequently, as the thickness of plate and shell becomes extremely thin, the shear strain energy predicted by the finite element analysis can be magnified unreasonably, even though the average value of the shear strain over the area tends to zero.

Finite element schemes for shell problems also suffer of the so-called membrane locking, i.e. the finite element approximation of the membrane component of the energy is unstable with respect to the thickness of the shell. The term membrane locking was coined by Stolarski and Belytschko (1981), who showed that it is related to an inadequate representation of inextensional modes. Later, Leino and Pitkäranta (1992, 1994) have analysed from a mathematical standpoint the membrane locking in a cylindrical shell problem and has shown that in the standard finite element methods locking occurs especially at low degrees of discretization. Several solutions to avoid the numerical locking have been proposed, mainly in the degenerate solid approach. Mixed formulations, reduced integration, and its offspring, selective reduced integration, have been often used to mitigate the effects of shear and membrane locking (Belytschko *et al.*, 1985; Bathe and Dvorkin, 1986; Bucalem and Bathe, 1993). Arnold and Brezzi (1997) deal with a mixed formulation of the Naghdi model, giving a family of locking free elements and proving the convergence of their numerical approach.

Our basic idea is that of combining the Naghdi model, more close to the description of the shell structure than the three-dimensional degenerate approach, with a displacement formulation. For the numerical approximation we consider a family of finite elements of hierarchic type, with degree ranging from one to four. The hierarchic structure allows the computation of a sequence of solutions, useful for the assessment of the overall performance of the finite elements. When the comparison between cost and accuracy is taken into account, high-order finite elements need a smaller computational effort to achieve the desired accuracy. In order to analyse the behavior of our finite elements respect to the membrane and shear locking, we have dealt with two test problems often used to assess the performance of numerical formulations based on the degenerated solid approach. The two tests are representative of extremely discriminating situations.

The first one is the well-known Scordelis–Lo problem. It is a membrane dominated problem and it is used to evaluate the ability of the shell elements to capture complex membrane state of stress. We have evaluated, among others, displacement and strain energy. The numerical results, especially for the elements of degree three and four, show a good agreement with all the available benchmark results.

The second test refers to a pinched cylindrical shell. It is a bending dominated problem and it is a severe test for a shell element performance with respect to both membrane and shear locking. The numerical results agree with the values known in the literature. Our numerical experiences indicate that high order elements perform very well in both the test problems.

The outline of the paper is the following. In Section 2, we describe the geometry of a thin shell, after introducing the deformation assumptions and the related deformation energy of the shell, we give the variational formulation of the Naghdi shell model. In Section 3, we describe the approximate problem and the family of hierarchic finite elements. In Section 4, we deal with the Naghdi formulation for cylindrical shells. The stiffness matrix, with all its components, is given. In Section 5, an extensive set of numerical results is presented.

2. THE NAGHDI SHELL MODEL

2.1. *Geometry of a thin shell*

Let $\mathbb{R}^3$ be the usual euclidean space (O, x_1, x_2, x_3) and let Ω be an open bounded subset of $\mathbb{R}^2$ with closure $\bar{\Omega}$. Let (ξ_1, ξ_2) denote a generic point of the set $\bar{\Omega}$. Let $\boldsymbol{\phi}$ be a smooth one-to-one mapping of $\bar{\Omega}$ into $\mathbb{R}^3$. The middle surface $\bar{S}$ of the shell (see Fig. 1) is the image in $\mathbb{R}^3$ of the set $\bar{\Omega}$ through the mapping $\boldsymbol{\phi}$.

$$\boldsymbol{\phi} = (\phi_1, \phi_2, \phi_3) : \bar{\Omega} \subset \mathbb{R}^2 \to \bar{S} \subset \mathbb{R}^3 \tag{1}$$

Thus we have $\bar{S} = \boldsymbol{\phi}(\bar{\Omega})$. Let us set $\mathbf{a}_\alpha = \boldsymbol{\phi}_{,\alpha} = \partial\boldsymbol{\phi}/\partial\xi_\alpha$ $(\alpha = 1, 2)$. the vectors $\mathbf{a}_1$, $\mathbf{a}_2$ are linearly independent at each point of $\bar{\Omega}$ and define the tangent plane to the midsurface $\bar{S}$ at each point $\boldsymbol{\phi}(\xi_1, \xi_2)$. Let $\mathbf{a}_3$ be the unit vector normal to the tangent plane. The set of vectors $\mathbf{a}_1$, $\mathbf{a}_2$, $\mathbf{a}_3$ define the covariant basis at the point $\boldsymbol{\phi}(\xi_1, \xi_2)$. The first fundamental form is $a_{\alpha\beta} = \boldsymbol{\alpha}_\alpha \cdot \mathbf{a}_\beta$, $(\alpha, \beta = 1, 2)$, with $a = \det(a_{\alpha\beta})$. Denoting by $a^{\alpha\beta}$ the components of the inverse matrix to $(a_{\alpha\beta})$, we introduce the contravariant basis $\mathbf{a}^\alpha = a^{\alpha\beta}\mathbf{a}_\beta$ and we set $\mathbf{a}^3 = \mathbf{a}_3$. The second fundamental form is $b_{\alpha\beta} = \mathbf{a}_3 \cdot \mathbf{a}_{\alpha,\beta} = \mathbf{a}_3 \cdot \mathbf{a}_{\beta,\alpha}$ and the following relation holds:

$$a^{\alpha\beta} \cdot b_{\beta\gamma} = b^\alpha_\gamma.$$

2.2. *The deformation assumptions*

Different mathematical models for shells have been proposed. The Naghdi model describes the deformation of a shell subject to a transverse loading when transverse shear deformation is taken into account. In Naghdi approach constant shear deformations are allowed across the thickness of the shell. The main assumption is that particles lying on the direction of the vector $\mathbf{a}_3$ remain on a straight line during deformation, but the line does not necessarily keep normal to the deformed middle surface. With such an assumption the vector $\mathbf{a}_3$ is allowed a rotation $\tilde{\theta}$ with covariant components θ_1, θ_2, i.e. $\tilde{\theta} = \theta_\alpha \mathbf{a}^\alpha$. Denoting by $\mathbf{a}_3^*$ the vector $\mathbf{a}_3$ after deformation, we have $\mathbf{a}_3^* = \mathbf{a}_3 + \theta_\alpha \mathbf{a}^\alpha$. In the model proposed by Naghdi the five unknowns are the covariant components u_i, $i = 1, 2, 3$, of the displacement

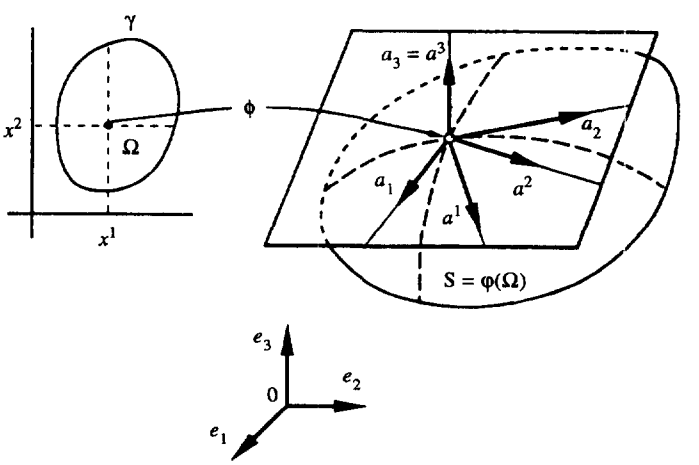

Fig. 1. Definition of the middle surface.

$\mathbf{u} = u_i \mathbf{a}^i$ of the points of the middle surface S of the shell and the two components θ_α of the rotation $\tilde{\theta}$ of the unit normal vector $\mathbf{a}_3$. Due to the mapping (1), the shell model reduces to a two-dimensional model and we search for a solution in the plane (ξ_1, ξ_2). This approach differs from the three-dimensional (3-D) degenerate model dealt with by many authors [see Bathe and Dvorkin (1986)], where isoparametric type transformations are taken into account.

2.3. *The strain energy*

For an arbitrary displacement field $\mathbf{u} \in (H^1(\Omega))^3$ and rotation field $\tilde{\theta} \in (H^1(\Omega))^2$, we define the change of curvature tensor $\boldsymbol{\Upsilon}$, the transverse shear strain tensor $\boldsymbol{\Sigma}$, the membrane strain tensor $\boldsymbol{\Lambda}$:

$$
\begin{aligned}
\boldsymbol{\Upsilon}_{\alpha\beta}(\mathbf{u}, \tilde{\theta}) &= \tfrac{1}{2}[\theta_{\alpha|\beta} + \theta_{\beta|\alpha} - b_\alpha^\gamma (u_{\gamma|\beta} - b_{\gamma\beta} u_3) - b_\beta^\gamma (u_{\gamma|\alpha} - b_{\gamma\alpha} u_3)] \\
&= \tfrac{1}{2}[\theta_{\alpha,\beta} + \theta_{\beta,\alpha} - b_\alpha^\gamma (u_{\gamma,\beta} - \Gamma_{\gamma\beta}^\delta u_\delta) - b_\beta^\gamma (u_{\gamma,\alpha} - \Gamma_{\gamma\alpha}^\delta u_\delta)] \\
&\quad + b_\alpha^\gamma b_{\gamma\beta} u_3 - \Gamma_{\alpha\beta}^\delta \theta_\delta \\
\boldsymbol{\Sigma}_\alpha(\mathbf{u}, \tilde{\theta}) &= u_{3|\alpha} + b_\alpha^\gamma u_\gamma + \theta_\alpha = u_{3,\alpha} + b_\alpha^\gamma u_\gamma + \theta_\alpha \\
\boldsymbol{\Lambda}_{\alpha\beta}(\mathbf{u}) &= \tfrac{1}{2}(u_{\alpha|\beta} + u_{\beta|\alpha}) - b_{\alpha\beta} u_3 = \tfrac{1}{2}(u_{\alpha,\beta} + u_{\beta,\alpha}) - \Gamma_{\alpha\beta}^\delta u_\delta - b_{\alpha\beta} u_3
\end{aligned} \tag{2}
$$

where $\Gamma_{\alpha\beta}^\delta = \Gamma_{\beta\alpha}^\delta = \mathbf{a}^\delta \cdot \mathbf{a}_{\beta,\alpha}$ is the Christoffel symbol and the vertical line denotes the covariant derivatives: $v_{\alpha|\beta} = v_{\alpha,\beta} - \Gamma_{\alpha\beta}^\delta v_\delta$, $v_{3|\beta} = v_{3,\beta}$.

Let us suppose that the shell is homogeneous and isotropic. As usual we denote by t, E and ν the thickness of the shell, the Young's modulus and the Poisson ratio, respectively. The shell is subject to external forces acting on the middle surface of the shell, whose resultant $\mathbf{p}$ can be written in terms of its covariant components p_i, i.e. $\mathbf{p} = p_i \mathbf{a}^i$. The shell is clamped on the subset of the boundary $\partial S_0 = \boldsymbol{\phi}(\Gamma_0) \times [-t/2, t/2]$, where $\Gamma_0 = \partial\Omega_0$ is a non-empty subset of $\partial\Omega$. The strain energy $\mathscr{E}$ of the shell can be written as the sum of three contributes: bending, shear and membrane energy. The energy functional has the following form:

$$
\begin{aligned}
\mathscr{E}(\mathbf{v}, \tilde{\psi}) &= \mathscr{E}^{\mathrm{B}}(\mathbf{v}, \tilde{\psi}) + \mathscr{E}^{\mathrm{S}}(\mathbf{v}, \tilde{\psi}) + \mathscr{E}^{\mathrm{M}}(\mathbf{v}) \\
\mathscr{E}^{\mathrm{B}}(\mathbf{v}, \tilde{\psi}) &= \frac{t^3}{2} \int_\Omega \frac{a^{\alpha\beta\gamma\delta}}{12} \Upsilon_{\alpha\beta}(\mathbf{v}, \tilde{\psi}) \boldsymbol{\Upsilon}_{\gamma\delta}(\mathbf{v}, \tilde{\psi}) \sqrt{a}\, \mathrm{d}\xi_1\, \mathrm{d}\xi_2 \\
\mathscr{E}^{\mathrm{S}}(\mathbf{v}, \tilde{\psi}) &= \frac{t}{2} \int_\Omega a^{\alpha\beta} \frac{E}{2(1+\nu)} \boldsymbol{\Sigma}_\alpha(\mathbf{v}, \tilde{\psi}) \boldsymbol{\Sigma}_\beta(\mathbf{v}, \tilde{\psi}) \sqrt{a}\, \mathrm{d}\xi_1\, \mathrm{d}\xi_2 \\
\mathscr{E}^{\mathrm{M}}(\mathbf{v}) &= \frac{t}{2} \int_\Omega a^{\alpha\beta\gamma\delta} \boldsymbol{\Lambda}_{\alpha\beta}(\mathbf{v}) \boldsymbol{\Lambda}_{\gamma\delta}(\mathbf{v}) \sqrt{a}\, \mathrm{d}\xi_1\, \mathrm{d}\xi_2
\end{aligned} \tag{3}
$$

with

$$
a^{\alpha\beta\gamma\delta} = \frac{E}{2(1+\nu)} \left[a^{\alpha\gamma} a^{\beta\delta} + a^{\alpha\delta} a^{\beta\gamma} + \frac{2\nu}{1-\nu} a^{\alpha\beta} a^{\gamma\delta} \right]. \tag{4}
$$

The load energy has the form

$$\mathscr{E}^{L}(\mathbf{v},\tilde{\psi}) = \int_{\Omega} \mathbf{p}\mathbf{v}\sqrt{a}\,d\xi_1\,d\xi_2. \tag{5}$$

Setting $\mathbf{f} = \mathbf{p}/t^3$ and scaling likewise the strain energy $\mathscr{E}$, the total energy functional can be written as:

$$\mathscr{E}^{T}(\mathbf{v},\tilde{\psi}) = \frac{1}{t^3}\mathscr{E}(\mathbf{v},\tilde{\psi}) - \int_{\Omega} \mathbf{f}\mathbf{v}\sqrt{a}\,d\xi_1\,d\xi_2. \tag{6}$$

According to the energy principle, the shell assumes a state of deformation such that the total energy $\mathscr{E}^{T}$ is minimized. We define $V = \{v \in H^1(\Omega) : v|_{\Gamma_0} = 0\}$ and $V^5 = \{\mathbf{v},\tilde{\psi}) : v_i, \psi_\alpha \in V\}$. The solution of the Naghdi model is the pair $(\mathbf{u},\tilde{\theta})$ such that:

$$(\mathbf{u},\tilde{\theta}) = \min_{(\mathbf{v},\tilde{\psi})\in V^5} \mathscr{E}^{T}(\mathbf{v},\tilde{\psi}). \tag{7}$$

When a variational form of eqn (7) is considered, the solution is the pair $(\mathbf{u},\tilde{\theta}) \in V^5$ such that:

$$\begin{cases} \displaystyle\int_{\Omega} \frac{a^{\alpha\beta\gamma\delta}}{12} \Upsilon_{\alpha\beta}(\mathbf{u},\tilde{\theta})\Upsilon_{\gamma\delta}(\mathbf{v},\tilde{\psi})\sqrt{a}\,d\xi_1\,d\xi_2 \\ \displaystyle + \frac{1}{t^2}\int_{\Omega} a^{\alpha\beta}\frac{E}{2(1+\nu)}\Sigma_{\alpha}(\mathbf{u},\tilde{\theta})\Sigma_{\beta}(\mathbf{v},\tilde{\psi})\sqrt{a}\,d\xi_1\,d\xi_2 \\ \displaystyle + \frac{1}{t^2}\int_{\Omega} a^{\alpha\beta\gamma\delta}\Lambda_{\alpha\beta}(\mathbf{u})\Lambda_{\gamma\delta}(\mathbf{v})\sqrt{a}\,d\xi_1\,d\xi_2 \\ \displaystyle = \int_{\Omega} \mathbf{f}\mathbf{v}\sqrt{a}\,d\xi_1\,d\xi_2 \quad \forall(\mathbf{v},\tilde{\psi}) \in V^5 \end{cases} \tag{8}$$

The previous problem is well posed, i.e. it has a unique solution [see Coutris (1978)]. The following uniqueness and existence theorem holds:

Theorem. Let $\boldsymbol{\phi} \in (C^3(\bar{\Omega}))^3$; let the measure of Γ_0 be >0, $\mathbf{p} \in (L^2(\Omega))^3$. Then problem (8) has a unique solution.

3. THE APPROXIMATE PROBLEM

3.1. *The discrete formulation*

Following the ideas explained in the previous paragraph, we solve the approximate problem on a plain domain. Let $\bar{\Omega}$ be a polygonal domain. Let us introduce a decomposition $\mathscr{T}_h$ of $\bar{\Omega}$ into quadrilateral elements $\mathscr{Q}_h$ such that $\cup_{\mathscr{Q}_h\in\mathscr{T}_h} \mathscr{Q}_h = \bar{\Omega}$. Let V_h be a finite dimensional space such that $V_h \subset V^5$. The approximate problem can be given the following form:

$$\begin{cases} \text{Find } (\mathbf{u}_h,\tilde{\theta}_h) \in V_h \quad \text{such that:} \\ \displaystyle\sum_{\mathscr{Q}_h\in\mathscr{T}_h}\int_{\mathscr{Q}_h} \frac{a^{\alpha\beta\gamma\delta}}{12}\Upsilon_{\alpha\beta}(\mathbf{u}_h,\tilde{\theta}_h)\Upsilon_{\gamma\delta}(\mathbf{v}_h,\tilde{\psi}_h)\sqrt{a}\,d\xi_1\,d\xi_2 \\ \displaystyle + \frac{1}{t^2}\sum_{\mathscr{Q}_h\in\mathscr{T}_h}\int_{\mathscr{Q}_h} a^{\alpha\beta}\frac{E}{2(1+\nu)}\Sigma_{\alpha}(\mathbf{u}_h,\tilde{\theta}_h)\Sigma_{\beta}(\mathbf{v}_h,\tilde{\psi}_h)\sqrt{a}\,d\xi_1\,d\xi_2 \\ \displaystyle + \frac{1}{t^2}\sum_{\mathscr{Q}_h\in\mathscr{T}_h}\int_{\mathscr{Q}_h} a^{\alpha\beta\gamma\delta}\Lambda_{\alpha\beta}(\mathbf{u}_h)\Lambda_{\gamma\delta}(\mathbf{v}_h)\sqrt{a}\,d\xi_1\,d\xi_2 \\ \displaystyle = \sum_{\mathscr{Q}_h\in\mathscr{T}_h}\int_{\mathscr{Q}_h} \mathbf{f}\mathbf{v}_h\sqrt{a}\,d\xi_1\,d\xi_2 \quad \forall(\mathbf{v}_h,\tilde{\psi}_h) \in V_h \end{cases} \tag{9}$$

3.2. *The finite elements for shells*

We observe that the shell model we deal with allows the use of two-dimensional finite elements. In recent papers [see Della Croce and Scapolla (1992a, 1992b)] a family of

Table 1. Number of shape functions for different degrees

Degree	Nodal s.f.	Side s.f.	Internal s.f.	Total # s.f.
1	4	—	—	4
2	4	4	—	8
3	4	8	—	12
4	4	12	1	17
...	...	...	...	...
p	4	$4(p-1)$	$\frac{1}{2}(p-2)(p-3)$	$4p+\frac{1}{2}(p-2)(p-3)$

hierarchic finite elements has been developed to deal with Reissner–Mindlin plate problems. The idea is to extend the features of such a family for the approximation of the shell problems, where also membrane energy is involved. The basic ideas of hierarchic finite elements are introduced in Babuška (1988), and Szabó and Babuška (1991). We remark that the hierarchic structure allows a consistent reduction of time in the computation of the stiffness matrix for the lower degree elements. Moreover, the solutions corresponding to different degrees for approximation can be usefully used for an assessment of the overall results. In the following we consider a family of finite elements with degrees varying from $p = 1$ to $p = 4$.

We consider the space

$$V_h = \{(\mathbf{v}_h, \tilde{\psi}_h) : (\mathbf{v}_h)_i, (\psi_h)_\alpha \in W_p(\mathcal{T}_h)\} \subset V^5 \tag{10}$$

where

$$W_p(\mathcal{T}_h) = \{w \in H^1(\Omega) : w|_{\mathcal{Q}_h} \in S_p(\mathcal{Q}_h) \quad \forall \mathcal{Q}_h \in \mathcal{T}_h\} \quad p = 1, 2, 3, 4 \tag{11}$$

and $S_p(\mathcal{Q}_h)$ is constructed as follows. Let $\mathcal{P}_p$ be the spaces of polynomials defined on the square $[-1, 1] \times [-1, 1]$ of degree less or equal p in the two variables. We take all monomials of the space $\mathcal{P}_p$ and we add the following monomial terms:

(a) the monomial $\{xy\}$ in the case $p = 1$;
(b) the monomials $\{x^p y, xy^p\}$ in the case $p \geq 2$.

The basis functions obtained in this way are the shape functions for the quadrilateral element. Referring to the classification of the shape functions suggested by Babuška (1988) as nodal, side and internal functions, in Table 1 we give the number of shape functions related to each unknown for general values of the degree p. We note that the following set of five degrees-of-freedom is associated to each node: $(\theta_1, \theta_2, u_1, u_2, u_3)$.

4. THE NAGHDI FORMULATION FOR CYLINDRICAL SHELLS

4.1. *The mathematical model*

Let us consider some model problems where the shape of the shell is cylindrical. In a system of Cartesian coordinates (O, x_1, x_2, x_3), the region occupied by the midsurface of the shell is:

$$S = \{(x_1, x_2, x_3) \in \mathbb{R}^3 : -L/2 < x_1 < L/2, x_2^2 + x_3^2 = R^2\} \tag{12}$$

where L and R are the length and the radius of the shell, respectively. Let us take a curvilinear coordinate system (ξ_1, ξ_2, ξ_3) placed at the centre of the upper part of the midsurface, and $\xi_1 = x_1$, $\xi_2 = R\theta$, $\theta \in [-\pi, \pi]$. The midsurface S of the shell is described by the mapping:

$$\boldsymbol{\phi}(\xi_1, \xi_2) : \bar{\Omega} \subset \mathbb{R}^2 \to \bar{S} \subset \mathbb{R}^3 \tag{13}$$

$$\begin{cases} \phi_1(\xi_1, \xi_2) = \xi_1 \\ \phi_2(\xi_1, \xi_2) = R \sin(\xi_2/R) \\ \phi_3(\xi_1, \xi_2) = R \cos(\xi_2/R) \end{cases} . \tag{14}$$

With such choices the region $\Omega \subset \mathbb{R}^2$ corresponding to the midsurface S is the rectangle:

$$\Omega = \{(\xi_1, \xi_2) : -L/2 < \xi_1 < L/2, -R\pi < \xi_2 < R\pi\}. \tag{15}$$

The geometrical features of the midsurface change as previously described. Under the previous geometrical assumptions the change of curvature tensor $\boldsymbol{\Upsilon}$, the transverse shear strain tensor $\boldsymbol{\Sigma}$, the membrane strain tensor $\boldsymbol{\Lambda}$ becomes as follows:

$$\begin{aligned} &\Upsilon_{11}(\mathbf{u}, \tilde{\theta}) = \theta_{1,1} \quad \Upsilon_{12}(\mathbf{u}, \tilde{\theta}) = \frac{1}{2}\left(\theta_{1,2} + \theta_{2,1} + \frac{1}{R} u_{2,1}\right) \\ &\Upsilon_{22}(\mathbf{u}, \tilde{\theta}) = \theta_{2,2} + \frac{1}{R}\left(u_{2,2} + \frac{1}{R} u_3\right) \\ &\Sigma_1(\mathbf{u}, \tilde{\theta}) = u_{3,1} + \theta_1 \quad \Sigma_2(\mathbf{u}, \tilde{\theta}) = u_{3,2} - \frac{1}{R} u_2 + \theta_2 \\ &\Lambda_{11}(\mathbf{u}) = u_{1,1} \quad \Lambda_{12}(\mathbf{u}) = \frac{1}{2}(u_{1,2} + u_{2,1}) \quad \Lambda_{22}(\mathbf{u}) = u_{2,2} + \frac{1}{R} u_3 \end{aligned} \tag{16}$$

Let us denote with $b(\mathbf{u}, \tilde{\theta}; \mathbf{v}, \tilde{\psi})$ the bilinear form associated to the bending component of the energy. We have:

$$\begin{aligned} b(\mathbf{u}, \tilde{\theta}; \mathbf{v}, \tilde{\psi}) = \frac{E}{24(1+\nu)} \int_\Omega \Bigg(&\frac{2}{1-\nu} \Upsilon_{11}(\mathbf{u}, \tilde{\theta}) \Upsilon_{11}(\mathbf{v}, \tilde{\psi}) \\ &+ \frac{2\nu}{1-\nu} \Upsilon_{22}(\mathbf{u}, \tilde{\theta}) \Upsilon_{11}(\mathbf{v}, \tilde{\psi}) + 4 \Upsilon_{\alpha\beta}(\mathbf{u}, \tilde{\theta}) \Upsilon_{\alpha\beta}(\mathbf{v}, \tilde{\psi}) \\ &+ \frac{2\nu}{1-\nu} \Upsilon_{11}(\mathbf{u}, \tilde{\theta}) \Upsilon_{22}(\mathbf{v}, \tilde{\psi}) + \frac{2}{1-\nu} \Upsilon_{22}(\mathbf{u}, \tilde{\theta}) \Upsilon_{22}(\mathbf{v}, \tilde{\psi}) \Bigg) \mathrm{d}\xi_1 \, \mathrm{d}\xi_2. \end{aligned} \tag{17}$$

Let us denote with $s(\mathbf{u}, \tilde{\theta}; \mathbf{v}, \tilde{\psi})$ the bilinear form associated to the shear component of the energy. We have:

$$s(\mathbf{u}, \tilde{\theta}; \mathbf{v}, \tilde{\psi}) = \frac{E}{2(1+\nu)} \int_\Omega (\Sigma_\alpha(\mathbf{u}, \tilde{\theta}) \Sigma_\alpha(\mathbf{v}, \tilde{\psi}) + \Sigma_\beta(\mathbf{u}, \tilde{\theta}) \Sigma_\beta(\mathbf{v}, \tilde{\psi})) \, \mathrm{d}\xi_1 \, \mathrm{d}\xi_2. \tag{18}$$

Let us denote with $m(\mathbf{u}, \mathbf{v})$ the bilinear form associated to the membrane component of the energy. We have:

$$\begin{aligned} m(\mathbf{u}, \mathbf{v}) = \frac{E}{2(1+\nu)} \int_\Omega \Bigg(&\frac{2}{1-\nu} \Lambda_{11}(\mathbf{u}) \Lambda_{11}(\mathbf{v}) + \frac{2\nu}{1-\nu} \Lambda_{22}(\mathbf{u}) \Lambda_{11}(\mathbf{v}) \\ &+ 4 \Lambda_{\alpha\beta}(\mathbf{u}) \Lambda_{\alpha\beta}(\mathbf{v}) + \frac{2\nu}{1-\nu} \Lambda_{11}(\mathbf{u}) \Lambda_{22}(\mathbf{v}) + \frac{2}{1-\nu} \Lambda_{22}(\mathbf{u}) \Lambda_{22}(\mathbf{v}) \Bigg) \mathrm{d}\xi_1 \, \mathrm{d}\xi_2. \end{aligned} \tag{19}$$

The variational formulation (8) assumes the following form:

$$\begin{cases} \text{Find } (\mathbf{u}, \tilde{\theta}) \in V^5 \quad \text{such that:} \\ b(\mathbf{u}, \tilde{\theta}; \mathbf{v}, \tilde{\psi}) + \dfrac{1}{t^2} s(\mathbf{u}, \tilde{\theta}; \mathbf{v}, \tilde{\psi}) + \dfrac{1}{t^2} m(\mathbf{u}, \mathbf{v}) = \displaystyle\int_\Omega \mathbf{f}\mathbf{v} \, d\xi_1 \, d\xi_2 \quad \forall (\mathbf{u}, \tilde{\psi}) \in V^5. \end{cases} \tag{20}$$

We remark that the formulation we have introduced differs from the one considered by Leino and Pitkäranta (1994) due to the extra term $1/R(u_{2,2} + (1/R)u_3)$ appearing in the component Υ_{22} of the curvature tensor.

4.2. *The stiffness matrix*

Let us give a matricial form of the approximation of problem (20). We consider a basis for the space $W_p(\mathcal{T}_h)$ and denote by $\mathbf{F}$ the corresponding vector of shape functions, i.e. $\mathbf{F} = (F_1, F_2, \ldots, F_N)$, where N is the dimension of the approximation space $W_p(\mathcal{T}_h)$. We can express the five unknown functions in terms of the functions F_i, $i = 1, \ldots, N$. We have:

$$\begin{aligned} \theta_1(\xi_1, \xi_2) &= \sum_{i=1}^{N} A_i F_i(\xi_1, \xi_2) = \mathbf{F} \cdot \mathbf{A} \\ \theta_2(\xi_1, \xi_2) &= \sum_{i=1}^{N} B_i F_i(\xi_1, \xi_2) = \mathbf{F} \cdot \mathbf{B} \\ u_1(\xi_1, \xi_2) &= \sum_{i=1}^{N} C_i F_i(\xi_1, \xi_2) = \mathbf{F} \cdot \mathbf{C} \\ u_2(\xi_1, \xi_2) &= \sum_{i=1}^{N} D_i F_i(\xi_1, \xi_2) = \mathbf{F} \cdot \mathbf{D} \\ u_3(\xi_1, \xi_2) &= \sum_{i=1}^{N} E_i F_i(\xi_1, \xi_2) = \mathbf{F} \cdot \mathbf{E}. \end{aligned} \tag{21}$$

We define the vectors

$$\mathbf{G} = [\mathbf{A}, \mathbf{B}, \mathbf{C}, \mathbf{D}, \mathbf{E}]^T \quad \mathbf{H} = [\mathbf{0}, \mathbf{0}, \mathbf{H}_1, \mathbf{H}_2, \mathbf{H}_3]^T \tag{22}$$

where

$$\mathbf{H}_i = \int_\Omega f_i \mathbf{F} \quad i = 1, 2, 3. \tag{23}$$

To compute the integrals we use $(p+1) \times (p+1)$ classical quadrature formulas of Gaussian type. The matrix form of the discrete problem assumes the following form:

$$\mathcal{K}\mathbf{G} = \mathbf{H} \tag{24}$$

where $\mathcal{K}$ denotes the stiffness matrix. The expression of the elementary stiffness matrix for an element $\mathcal{Q}_h \in \mathcal{T}_h$ is given in Fig. 2, where the following notations have been used:

$$\begin{aligned} \mathbf{B} &= \int_{\mathcal{Q}_h} \mathbf{F}^T \mathbf{F} \, dx \, dy \\ \mathbf{B}_x &= \int_{\mathcal{Q}_h} \mathbf{F}^T \mathbf{F}_{/x} \, dx \, dy \quad \mathbf{B}_y = \int_{\mathcal{Q}_h} \mathbf{F}^T \mathbf{F}_{/y} \, dx \, dy \\ \mathbf{B}_{xx} &= \int_{\mathcal{Q}_h} \mathbf{F}_{/x}^T \mathbf{F}_{/x} \, dx \, dy \quad \mathbf{B}_{yy} = \int_{\mathcal{Q}_h} \mathbf{F}_{/y}^T \mathbf{F}_{/y} \, dx \, dy \\ \mathbf{B}_{xy} &= \int_{\mathcal{Q}_h} \mathbf{F}_{/x}^T \mathbf{F}_{/y} \, dx \, dy \quad \mathbf{B}_{yx} = \int_{\mathcal{Q}_h} \mathbf{F}_{/y}^T \mathbf{F}_{/x} \, dx \, dy \end{aligned} \tag{25}$$

$$
K_e = \begin{bmatrix}
C_b\left[\mathbf{B}_{xx} + \frac{1-\nu}{2}\mathbf{B}_{yy}\right] + C_s\mathbf{B} & C_b\left[\nu\mathbf{B}_{xy} + \frac{1-\nu}{2}\mathbf{B}_{yx}\right] & 0 & C_b\left[\frac{\nu}{R}\mathbf{B}_{xy} + \frac{1-\nu}{2R}\mathbf{B}_{yx}\right] & C_b\frac{\nu}{R^2}\mathbf{B}_x + C_s\mathbf{B}_x{}^T \\
 & C_b\left[\frac{1-\nu}{2}\mathbf{B}_{xx} + \mathbf{B}_{yy}\right] + C_s\mathbf{B} & 0 & C_b\left[\frac{1}{R}\mathbf{B}_{yy} + \frac{1-\nu}{2R}\mathbf{B}_{xx}\right] - \frac{1}{R}C_s\mathbf{B} & C_b\frac{1}{R^2}\mathbf{B}_y{}^T + C_s\mathbf{B}_y \\
 & & C_m\left[\mathbf{B}_{xx} + \frac{1-\nu}{2}\mathbf{B}_{yy}\right] & C_m\left[\nu\mathbf{B}_{xy} + \frac{1-\nu}{2}\mathbf{B}_{yx}\right] & C_m\frac{\nu}{R}\mathbf{B}_x \\
 & & & C_b\left[\frac{1}{R^2}\mathbf{B}_{yy} + \frac{1-\nu}{2R^2}\mathbf{B}_{xx}\right] + C_m\left[\mathbf{B}_{yy} + \frac{1-\nu}{2}\mathbf{B}_{xx}\right] + C_s\frac{1}{R^2}\mathbf{B} & C_b\frac{1}{R^2}\mathbf{B}_y - \frac{1}{R}C_s\mathbf{B}_y{}^T + C_m\frac{1}{R}\mathbf{B}_y \\
\text{symmetric} & & & & C_b\frac{1}{R^2}\mathbf{B} + C_m\frac{1}{R^2}\mathbf{B} + C_s\left[\mathbf{B}_{xx} + \mathbf{B}_{yy}\right]
\end{bmatrix}
$$

Fig. 2. The stiffness matrix $\mathcal{K}_e$.

and

$$C_b = \frac{E}{12(1-\nu^2)}, \quad C_s = \frac{Et^{-2}}{2(1+\nu)}, \quad C_m = \frac{Et^{-2}}{1-\nu^2}. \tag{26}$$

5. NUMERICAL RESULTS

The model we have introduced, unlike the 3-D degenerate approach, does not involve an approximation of the geometry of the shell and it describes the curvature of the shell more accurately than in the model suggested by Leino and Pitkäranta. However the locking phenomenon is still present. Our basic idea is that of combining such a model, more close to the description of the shell structure, with a simple displacement formulation. The hierarchic structure of the finite elements allows us to increase the degree of approximation without using more sophisticated formulations or special numerical techniques, as it is usually done. We analyse the reliability of the model together with the finite element scheme, and we compare the numerical results with the ones obtained in the 3-D degenerate approach [see Bucalem and Bathe (1993)].

In this direction we consider two classical test problems. These problems are discriminating [see Belytschko *et al.* (1985); Ibrahimbegovic and Frey (1994)] to test the performance of the finite elements. We consider the Scordelis–Lo problem (Scordelis and Lo, 1964) and the pinched cylinder with a diaphragm (Flügge, 1973). The Scordelis–Lo problem is extremely useful for determining the ability of an element to accurately solve complex states of membrane strain. A substantial part of the strain energy is membrane strain energy so the representation of inextensional bending modes is not crucial in this problem. The pinched cylinder with a diaphragm is one of the most severe tests for both inextensional bending modes and complex membrane states. We briefly describe each of the two test problems.

5.1. *Scordelis–Lo problem*

The problem deals with a cylindrical shell known in the literature as barrel vault. The shell is described in Fig. 3. This typical shell is used in civil engineering using conventional processes by Scordelis and Lo (1964). The essential features of such example can be also found in Zienkiewicz and Taylor (1989, 1991), Bathe and Dvorkin (1986). The shell is simply-supported on rigid diaphgrams and is free on the other sides. The shell is loaded by its own weight P. The barrel vault is a portion of cylindrical shell, with midsurface described as follows:

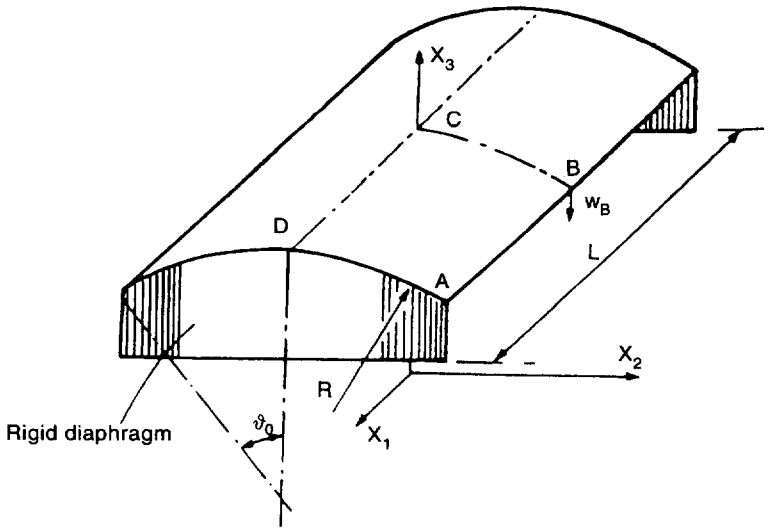

Fig. 3. Scordelis–Lo roof.

$$S = \{(x_1, x_2, x_3) \in \mathbb{R}^3 : -L/2 < x_1 < L/2,$$
$$-R\sin(2\pi/9) < x_2 < R\sin(2\pi/9), x_3 > 0, x_2^2 + x_3^2 = R^2\}. \quad (27)$$

Applying the mapping (13) and (14) we get the following expression for Ω:

$$\Omega = \{(\xi_1, \xi_2) : -L/2 < \xi_1 < L/2, -R2\pi/9 < \xi_2 < R2\pi/9\}. \quad (28)$$

The physical data given in Table 2 have been assumed.

The covariant components of the vertical load are: $p_1 = 0$, $p_2 = -P\sin(\xi_2/R)$, $p_3 = P\cos(\xi_2/R)$. The barrel vault has a symmetric structure. Thus, the computations have been performed only on a quarter of the shell, using a uniform decomposition. The following symmetry conditions have been assumed:

$$u_2(\xi_1, 0) = \theta_2(\xi_1, 0) = 0$$
$$u_1(0, \xi_2) = \theta_1(0, \xi_2) = 0 \quad (29)$$

and the following boundary conditions are prescribed

$$u_2(L/2, \xi_2) = u_3(L/2, \xi_2) = \theta_2(L/2, \xi_2) = 0. \quad (30)$$

For each test, among others, displacement at the midpoint B of the free edge and the strain energy have been computed. Let $u_3^{ex}(B)$ denote the exact displacement at the point B of the shell and $u_3(B)$ the finite element solution. The relative displacement error is defined as

Table 2. Physical data

Quantity	Name	Value
Young's modulus	E	4.32×10^8 lb/ft^2
Poisson's ratio	ν	0.0
thickness	t	0.25 ft
radius	R	25 ft
length	L	50 ft
angle	θ_0	$2\pi/9$ rad
load	P	90 lb/ft^2

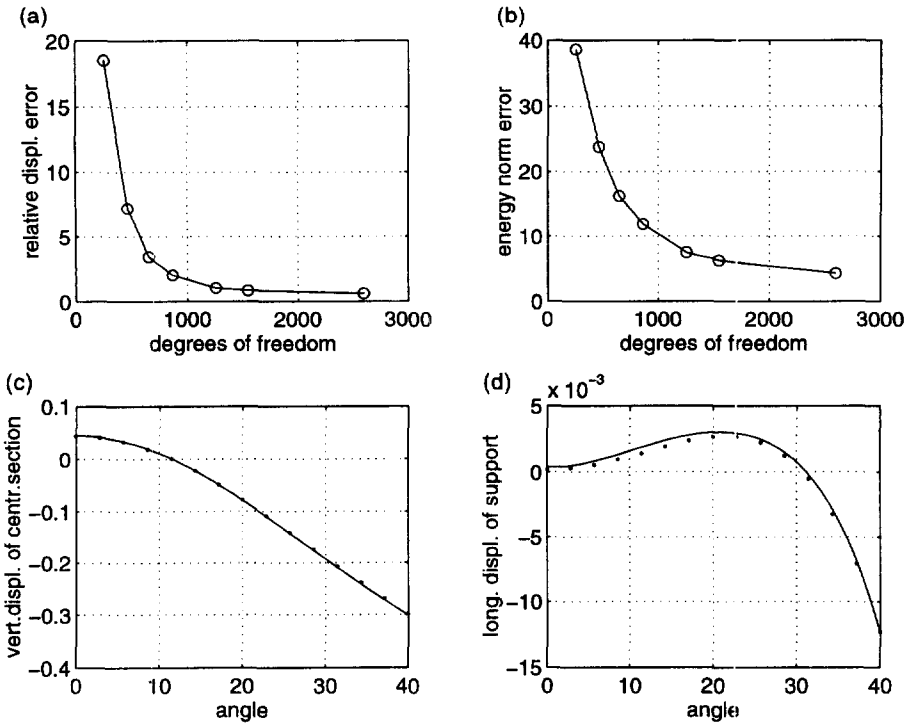

Fig. 4. (a) Relative displacement error vs degrees-of-freedom for $p = 2$; (b) energy norm error vs degrees-of-freedom for $p = 2$; (c) vertical displacement of the central section vs angle of the roof for $p = 2$; (d) longitudinal displacement of support vs angle of the roof for $p = 2$.

$$DE\% = [(u_3^{ex}(B) - u_3(B))/u_3^{ex}(B)] \times 100. \tag{31}$$

The exact strain energy is not available. Out of the discrete strain energy an extrapolation has been made in order to get an accurate value of the energy. Let E_{ex} denote such a energy, let E_h be the discrete energy. We consider the energy norm error defined as

$$EE\% = [(E_{ex} - E_h)/E_{ex}]^{1/2} \times 100. \tag{32}$$

In Table 3 the normalized displacement, i.e. the ratio between computed and exact solutions [see McNeal and Harder (1985)], is shown for several decompositions. We observe that the performance is very poor for $p = 1$. Reliable results are obtained for $p = 2$ only with a substantially high number of degrees-of-freedom. For $p = 3$ and $p = 4$ the exhibited performances are good even for low number of degrees-of-freedom. The results obtained by our elements are competitive with respect to the available benchmark results.

In Figs 4–6 we report some numerical results. The results in the first set of drawings have been obtained using the finite element of degree $p = 2$. Figure 4(a) shows the relative

Table 3. Degrees-of-freedom and related normalized displacement at point B for $p = 1, 2, 3, 4$

d.o.f.	$p=1$ $\frac{u_3(B)}{u_3^{ex}(B)}$	d.o.f.	$p=2$ $\frac{u_3(B)}{u_3^{ex}(B)}$	d.o.f.	$p=3$ $\frac{u_3(B)}{u_3^{ex}(B)}$	d.o.f.	$p=4$ $\frac{u_3(B)}{u_3^{ex}(B)}$
60	0.0332	255	0.8149	230	0.9343	345	0.9945
175	0.0694	395	0.9277	410	0.9881	625	0.9948
585	0.1342	650	0.9653	755	0.9940	1165	0.9951
825	0.1456	865	0.9795	1060	0.9946	2205	0.9954
1105	0.1742	1255	0.9895	1415	0.9949	3565	0.9958
—	—	2595	0.9938	2540	0.9954	—	—

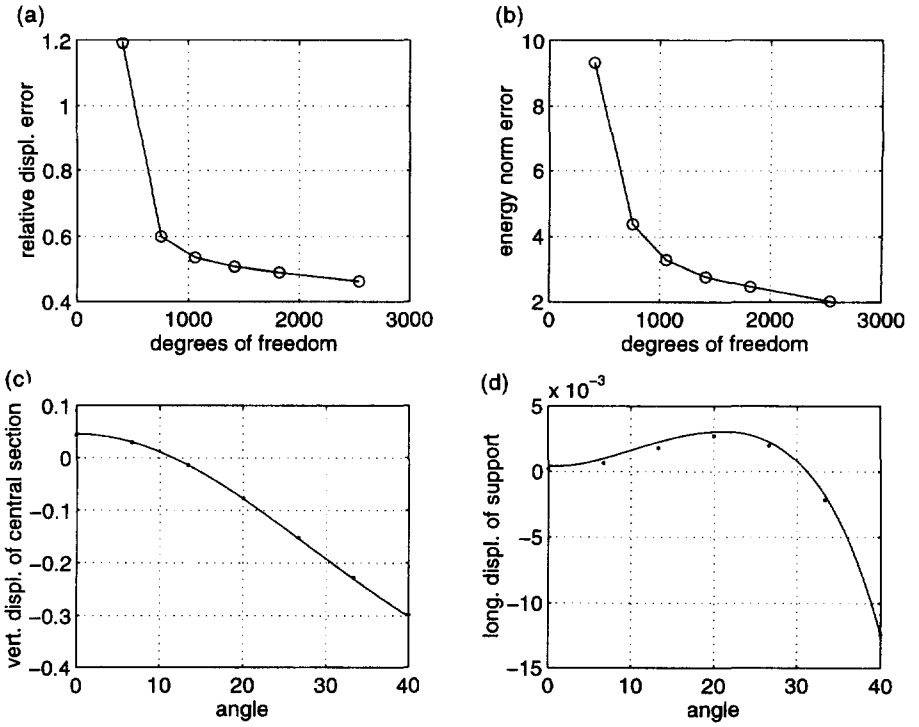

Fig. 5. (a) Relative displacement error vs degrees-of-freedom for $p = 3$; (b) energy norm error vs degrees-of-freedom for $p = 3$; (c) vertical displacement of the central section vs angle of the roof for $p = 3$; (d) longitudinal displacement of support vs angle of the roof for $p = 3$.

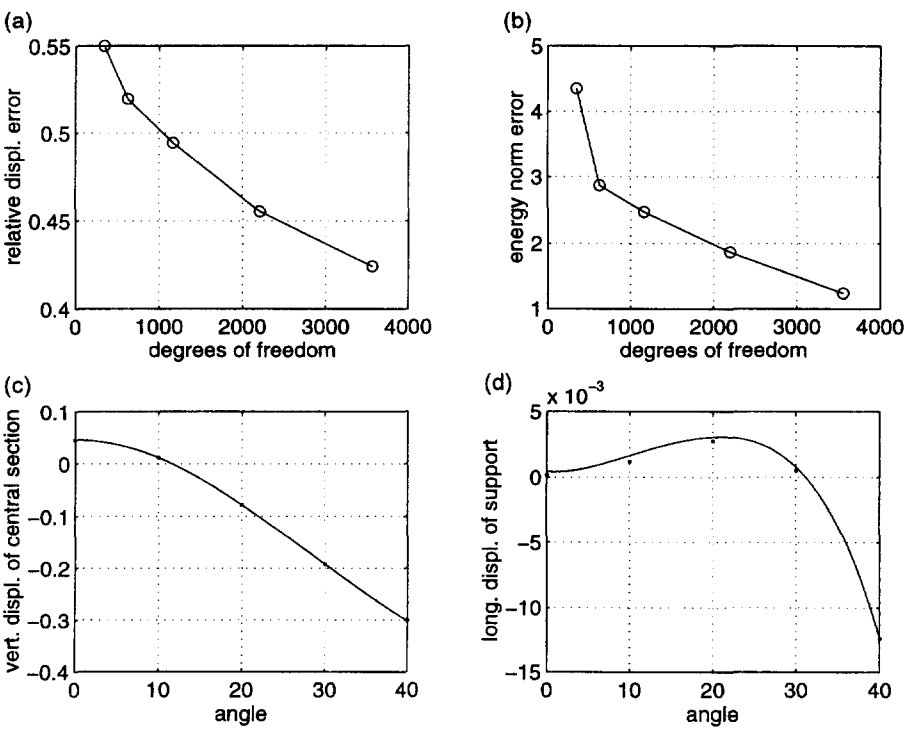

Fig. 6. (a) Relative displacement error vs degrees-of-freedom for $p = 4$; (b) energy norm error vs degrees-of-freedom for $p = 4$; (c) vertical displacement of the central section vs angle of the roof for $p = 4$; (d) Longitudinal displacement of support vs angle of the roof for $p = 4$.

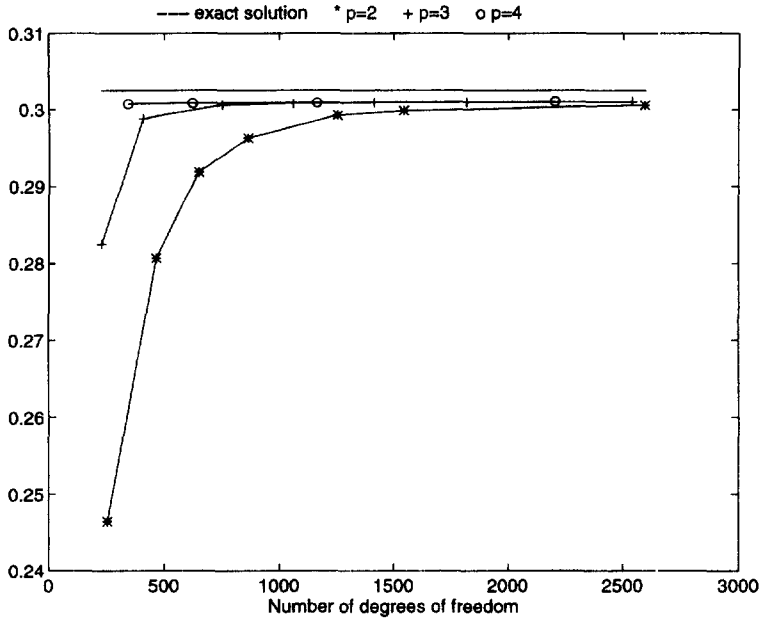

Fig. 7. Barrel vault test: computed displacement at the point B (exact solution: 0.3024 ft).

normal displacement error at the point B vs the number of degrees-of-freedom (d.o.f.). Figure 4(b) shows the energy norm error vs the number of degrees-of-freedom. In Fig. 4(c) we report, for a prescribed mesh, the vertical displacement along the central section of the shell vs the angle θ. The decomposition is 9×7 with 1110 d.o.f. Figure 4(d) shows, for the same mesh, the longitudinal displacement along the support vs the angle θ.

In Figures 5(a–d) and 6(a–d) the same results are given for the element of degree $p = 3$ and $p = 4$, respectively. Figures 5(c,d) is related to a mesh 4×3, corresponding to 410 d.o.f., and the Figure 6(c, d) is related to 3×2 mesh, corresponding to 345 d.o.f. We note that, both in the case of the relative normal displacement error and in the energy norm error, a good rate of convergence is achieved if high-order are employed. The results in Figures 4(c, d), 5(c, d) and 6(c, d) show an excellent convergence of the discrete solution to the expected solution given by Zienkiewicz and Taylor (1991), even if coarse meshes are used, especially for $p = 3$ and $p = 4$ elements. In Fig. 7, we show the behavior of the computed displacement at the point B, compared with the exact value, against the number of degrees-of-freedom, for $p = 2, 3, 4$.

5.2. *Pinched cylindrical shell*

The second test we consider is the one called pinched shell. This structure has been analyzed in Bathe and Ho (1981), Belytschko *et al.* (1985) and the essential shapes are shown in Fig. 8. The pinched shell is simply supported at each end by rigid diaphragm and singularly loaded by two opposed forces acting at midpoint of the shell. Due to the symmetry of the structure the computations have been performed, using a uniform decomposition, on a octave of the shell. Such a domain is described as

$$S = \{(x_1, x_2, x_3) \in \mathbb{R}^3 : 0 < x_1 < L/2, 0 < x_2 < R, x_2^2 + x_3^2 = R^2\} \tag{33}$$

corresponding to the rectangle

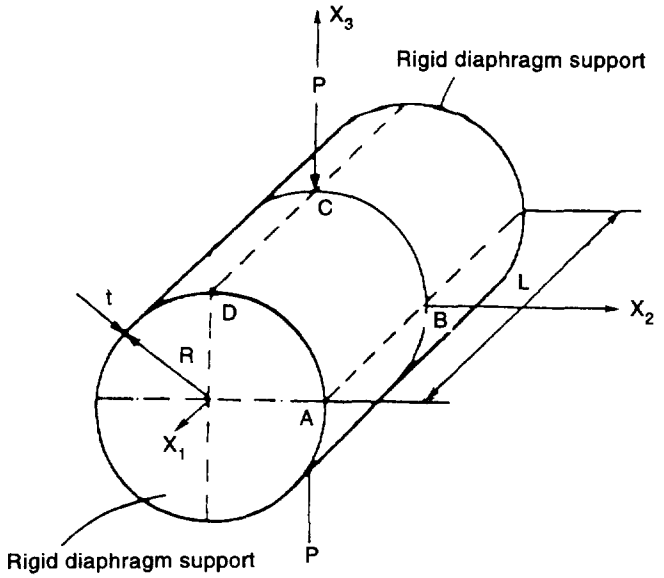

Fig. 8. The pinched cylinder.

$$\Omega = \{(\xi_1, \xi_2) : 0 < \xi_1 < L/2, 0 < \xi_2 < R\pi/2\}. \tag{34}$$

The physical data given in Table 4 have been assumed.

The following symmetry conditions are assumed:

$$\begin{aligned} u_2(\xi_1, 0) &= \theta_2(\xi_1, 0) = 0 \\ u_1(0, \xi_2) &= \theta_1(0, \xi_2) = 0 \\ u_2(\xi_1, R\pi/2) &= \theta_2(\xi_1, R\pi/2) = 0 \end{aligned} \tag{35}$$

and the following boundary conditions are prescribed

$$u_2(L/2, \xi_2) = u_3(L/2, \xi_2) = \theta_2(L/2, \xi_2) = 0. \tag{36}$$

In Table 5 the normalized displacement, i.e. the ratio between computed and exact solution [0.18248×10^{-4}, Flügge (1973)], at the loaded point C is presented for several decompositions. We can see that all the tested finite elements work reasonably well, with only the element of degree $p = 2$ converging slowly.

Table 4. Physical data for pinched shell

Quantity	Name	Value
Young's modulus	E	3×10^6 psi
Poisson's ratio	ν	0.3
thickness	t	3 in
radius	R	300 in
length	L	600 in
load	P	1 lb

Table 5. Degrees-of-freedom and related normalized displacement at point C for $p = 2, 3, 4$

d.o.f.	$p = 2$ $\frac{u_3(C)}{u_3^{ex}(C)}$	d.o.f.	$p = 3$ $\frac{u_3(C)}{u_3^{ex}(C)}$	d.o.f.	$p = 4$ $\frac{u_3(C)}{u_3^{ex}(C)}$
105	0.0443	165	0.1892	245	0.4737
480	0.3400	780	0.7971	805	0.8525
1705	0.7586	1845	0.9329	1685	0.9404
2405	0.8321	2805	0.9628	2885	0.9745

In Fig. 9(a, b) we consider the element of degree $p = 2$ and we show the behavior of the quantity Etu_3/p along the central lines DC and BC, respectively. Figure 9(c) shows the quantity Etu_1/p along the rigid diaphragm. The mesh 10×10 with 1705 d.o.f. is used. In Figs 10(a–c) and 11(a–c) we report the same results for the elements of degree $p = 3$ and $p = 4$, respectively. The meshes are 8×8 for the element of degree 3 (1845 d.o.f.) and 6×6 for the element of degree 4 (1685 d.o.f.). In Fig. 12, we show the behavior of normalized displacement at the point C for our elements of degree $p = 3$ and $p = 4$, compared with the solution obtained solving the 3-D degenerate model with the classical 16-node displacement based shell element (Bucalem and Bathe, (1993). This element makes use of a complete space of polynomials of degree 3, i.e. 16 degrees-of-freedom, while the corresponding element of degree 3 in our family uses only 12 degrees-of-freedom. We use as index of mesh refinement the number of nodes per side. It can be seen from the figure that both the elements of degree $p = 3$ and $p = 4$ show good convergence properties and perform better than the classical 16-node element.

6. CONCLUDING REMARKS

The numerical solution of thin Naghdi shell model with hierarchic finite elements has been considered. The results show that good performances are achieved by using high-order finite elements to solve the shell problem in its displacement formulation. The numerical results exhibit a good agreement with the values known in the literature. Our numerical

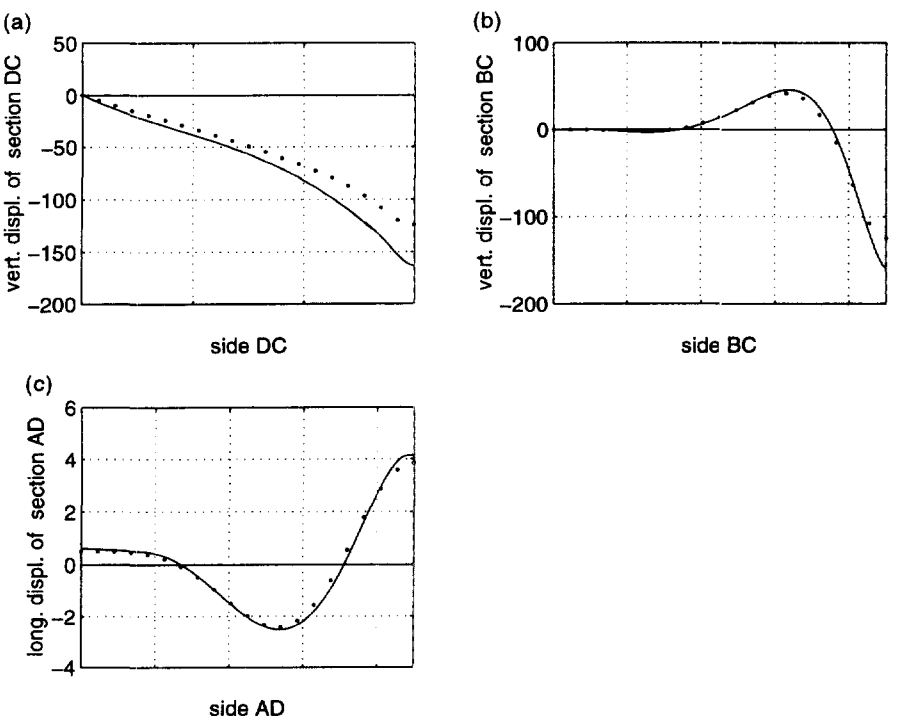

Fig. 9. (a) Vertical displacement of section DC vs side DC for $p = 2$; (b) vertical displacement of section BC vs side BC for $p = 2$; (c) longitudinal displacement of section AD vs side AD for $p = 2$.

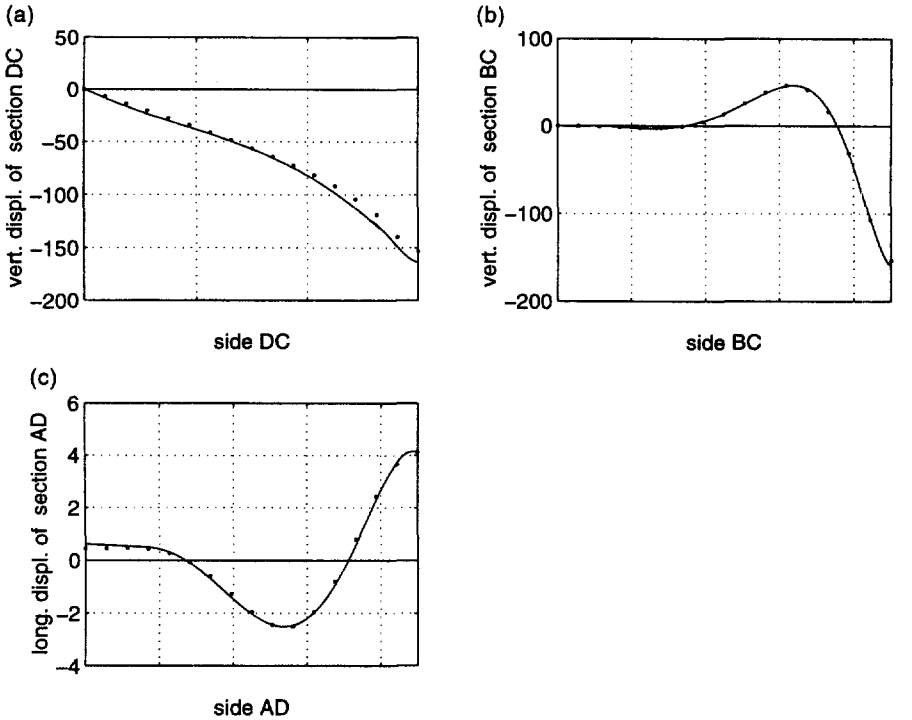

Fig. 10. (a) Vertical displacement of section DC vs side DC for $p = 3$; (b) vertical displacement of section BC vs side BC for $p = 3$; (c) longitudinal displacement of section AD vs side AD for $p = 3$.

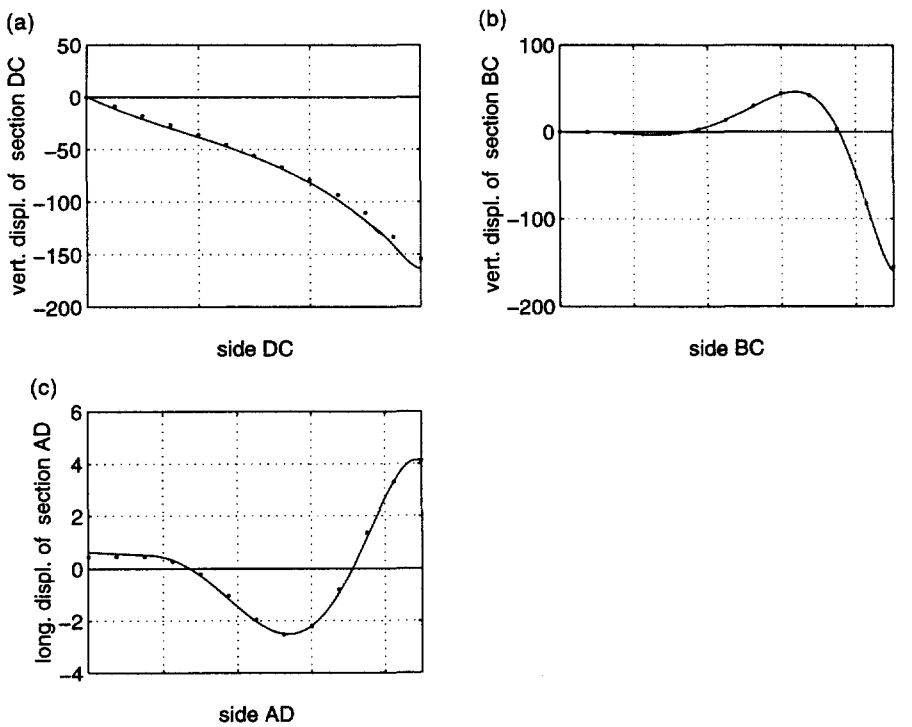

Fig. 11. (a) Vertical displacement of section DC vs side DC for $p = 4$; (b) vertical displacement of section BC vs side BC for $p = 4$; (c) longitudinal displacement of section AD vs side AD for $p = 4$.

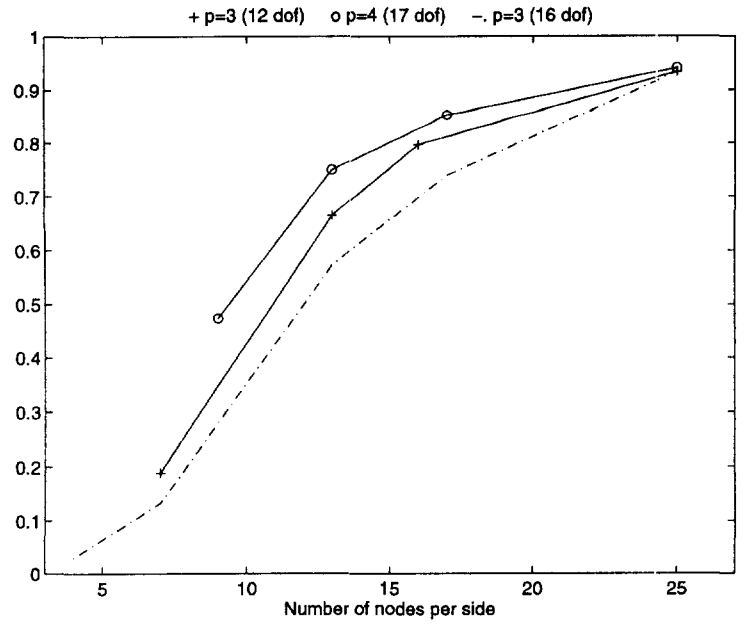

Fig. 12. Normalized displacement for the serendipity elements of degree $p = 3$ and $p = 4$ and the complete element of degree $p = 3$.

experiences, especially for the elements of degree 3 and 4, indicate that high-order elements perform very well in both the test problems and match all the available benchmark results. We observe that only rectangular decompositions have been considered in our numerical works. It is known that distorted elements increase the computational error, especially for low degree elements. Cost analysis should also be taken into account to compare the performance of the different elements. We observe that the hierarchic structure allows a low cost computation of a sequence of solutions useful to assess the quality of the numerical results.

REFERENCES

Ahmad, S., Irons, B. M. and Zienkiewicz, O. C. (1970) Analysis of thick and thin shell structures by curved finite elements. *International Journal for Numerical Methods Engineering* **2,** 419–451.

Antman, S. S. (1976) Ordinary differential equations of nonlinear elasticity, Part I: foundations of the theory of non-linearly elastic rods and shells. *Archive for Rational Mechanical Analysis* **61,** 307–351.

Arnold, D. N. and Brezzi, F. (1997) Locking free finite elements for shells. *Mathematics of Computation* (in press).

Babuška, I. (1988). The p and h–p versions of the finite element method. *Finite Elements: Theory and Application*, The state of the art. In eds. D. L. Dwoyer, M. Y. Hussaini and R. G. Voigt. Springer, New York, pp. 199–239.

Bathe, K.-J. (1982) *Finite Element procedures in Engineering Analysis.* Prentice-Hall, Englewood Cliffs, N.J.

Bathe, K.-J. and Ho, L. W. (1981) A simple and effective element for analysis of general shell structures. *Computers and Structures,* **13,** 673–681.

Bathe, K.-J. and Dvorkin, E. N. (1986) A formulation of general shell elements. The use of mixed interpolation of tensorial components. *International Journal for Numerical Methods in Engineering,* **22,** 697–722.

Belytschko, T., Stolarski, H., Liu, W. K., Carpenter, N. and Ong, J. S.-J. (1985) Stress projection for membrane and shear locking in shell finite elements. *Computational Methods in Applied Mechanical Engineering* **51,** 221–258.

Bernadou, M. (1994) *Méthodes d'Éléments Finis pour les Problèmes de Coque Mince.* Masson, Paris.

Bernadou, M. and Boisserie, J. M. (1982) *The Finite Element Method in Thin Shell Theory: Applications to Arch Dam Simulations.* Birkhauser, Boston.

Bucalem, M. L. and Bathe, K.-J. (1993) High-order MITC general shell elements. *International Journal for Numerical Methods of Engineering* **36,** 3729–3754.

Cosserat, E. and Cosserat, F. (1909) *Théorie des Corps Déformables.* Hermann, Paris, pp. 953–1173.

Coutris, N. (1978) Théorème d'existence et d'unicité pour problème de coque élastique dans le cas d'un modèle linéaire de P. M. Naghdi. *RAIRO Analyse Numérique* **12,** 51–57.

Della Croce, L. and Scapolla, T. (1992a) High-order finite elements for thin to moderately thick plates. *Computational Mechanics* **10,** 263–279.

Della Croce, L. and Scapolla, T. (1992b) Hierarchic finite elements with selective and uniform reduced integration for Reissner–Mindlin plates. *Computational Mechanics* **10,** 121–131.

Flügge, W. (1973) *Stresses in Shells* 2nd edn. Springer, Berlin.

Hughes, T. J. R. (1987) *The Finite Element Method.* Prentice-Hall, Englewood Cliffs, N.J.

Ibrahimbegovic, A. and Frey, F. (1994) Stress resultant geometrically non-linear shell theory with drilling rotations, Part III : linearized kinematics. *International Journal for Numerical Methods of Engineering* **37,** 3659–3683.

Koiter, W. T. (1970) On the foundations of the linear theory of thin elastic shell. *Proceedings of the Koninklijke Nederlandse Akademie van Wetenschappen* **B73,** 169–195.

Leino, Y. and Pitkäranta, J. (1994) On the membrane locking of h–p finite elements in a cylindrical shell problem. *International Journal for Numerical Methods of Engineering* **37,** 1053–1070.

Liu, W. K., Law, E. S., Lam, D. and Belytschko, T. (1966) Resultant-stress degenerate-shell element. *Computational Methods in Applied Mechanical Engineering* **55,** 259–300.

MacNeal, R. H. and Harder, R. L. (1985) A proposed standard set of problems to test finite element accuracy. *Finite Elements in Analysis and Design* **1,** 3–20.

Naghdi, P. M. (1963) Foundations of elastic shell theory. *Progress in Solid Mechanics.* Vol. 4, pp. 1–90. North-Holland, Amsterdam.

Naghdi, P. M. (1972) The theory of shells and plates. In *Handbuch der Physik*, Vol. VI. pp. 425–640, Springer, Berlin.

Pitkäranta, J. (1992) The problem of membrane locking in finite element analysis of cylindrical shells. *Numerische Mathematik* **61,** 523–542.

Ramm, E. (1977) A plate/shell element for large deflection and rotations. In *Formulations and Computational Algorithms in Finite Element Analysis* eds K.-J. Bathe, J. T. Oden and W. Wunderlich. MIT Press, Cambridge.

Scordelis, A. C. and Lo, K. S. (1964) Computer analysis in cylindrical shells. *Journal of American Concrete Institute* **61,** 561–593.

Simo, J. C. and Fox, D. D. (1989a) On stress resultant geometrically exact shell model. Part. I : formulation and optimal parametrization. *Computational Methods in Applied Mechanical Engineering* **72,** 267–304.

Simo, J. C., Fox, D. D. and Rifai, M. S. (1989b) On stress resultant geometrically exact shell model. Part. II : the linear theory. Computational aspects. *Computational Methods in Applied Mechanical Engineering* **73,** 53–92.

Simo, J. C., Fox, D. D. and Rifai, M. S. (1990) On stress resultant geometrically exact shell model. Part. III : computational aspects of the nonlinear theory. *Computational Methods in Applied Mechanical Engineering* **79,** 21–70.

Stolarski, H. and Belytschko, T. (1981) Reduced integration for shallow-shell facet elements. In *New Concepts in Finite Element Analysis*, eds. T. J. R. Hughes, D. Gartling and R. L. Spilker. ASME, New York.

Szabó, B. and Babuška, I. (1991) *Finite Element Analysis.* Wiley, New York.

Zienkiewicz, O. C. and Taylor, R. L. (1989, 1991) *The Finite Element Method*, Vols 1 and 2. McGraw-Hill, London.